Applied Catalysis B: Environmental 303 (2022) 120848

Contents lists available at ScienceDirect

Applied Catalysis B: Environmental

journal homepage: www.elsevier.com/locate/apcatb

Anodic production of hydrogen peroxide using commercial carbon materials

Dhananjai Pangotra [a,b], Lénárd-István Csepei [a], Arne Roth [a], Carlos Ponce de León [c], Volker Sieber [a,b], Luciana Vieira [a,*]

[a] Fraunhofer Institute of Interfacial Engineering and Biotechnology IGB, Bio-, Electro-, and Chemocatalysis BioCat, Straubing Branch, Schulgasse 11a, 94315, Straubing, Germany

[b] Chair of Chemistry for Biogenic Resources, Campus Straubing for Biotechnology and Sustainability, Technical University of Munich, Schulgasse 16, 94315, Straubing, Germany

[c] Electrochemical Engineering Laboratory, Faculty of Engineering and Physical Sciences, University of Southampton, Highfield, Southampton SO17 1BJ, United Kingdom

ARTICLE INFO

Keywords:
Carbon anodes
Electrocatalysis
Hydrogen peroxide
Anodic H_2O_2 production
Water oxidation

ABSTRACT

The electrochemical production of hydrogen peroxide (H_2O_2) from water is an appealing alternative to substitute the classic anthraquinone process. Herein, we show a process development to maximize the efficiency of the anodic production of H_2O_2. Carbon materials were used as anodes to optimize process parameters such as current density, electrolyte concentration, and the pH. We found that the electrolyte concentration, pH, and the presence of a chemical stabilizer have a substantial effect on the selectivity of water oxidation to H_2O_2. The addition of Na_2SiO_3 as a stabilizer increased the H_2O_2 production significantly at high pH regimes. A direct relationship between CO_3^{2-} ion activity and enhanced production of H_2O_2 was also observed. We report H_2O_2 concentrations in the anolyte up to 33 mmol L^{-1} at a current density of 100 mA cm^{-2} using commercial and low-cost carbon fiber paper.

1. Introduction

Hydrogen peroxide (H_2O_2) is a widely used industrial product. Because its decomposition generates oxygen (O_2) and water (H_2O) only, it is widely praised as a "green oxidant". It is used as an oxidizing agent in the chemical industry [1–3], in wastewater treatment [4,5], and as a propellant in the aerospace industry [6–8]. In refineries, H_2O_2 is applied for oxidative desulfurization of oil fractions to meet regulations referring to transportation fuels [9–13]. Changes in the limit of sulfur established by the International Maritime Organization (IMO) may lead to an exponential increase in H_2O_2 demand in this sector [14–16]. H_2O_2 also has a biocidal effect [17], thus it is used in low concentrations as a component of antiseptics [18] and hand sanitizers certified by the World Health Organization [19]. Recent research shows its promising results in the disinfection of personal protective equipment against the SARS-CoV-2 and COVID-19 virus [20–22]. While the healthcare industry's application was considered a relatively minor market, after the outbreak of COVID-19, the H_2O_2 demand in this branch increased dramatically [23].

Currently, H_2O_2 is produced via the anthraquinone (AO) process, an energy-demanding multistep method that requires large quantities of harmful organic solvents and fossil-based hydrogen [24,25]. Therefore, developing an alternate "green" route for H_2O_2 production is a subject of high scientific and economic interest [13]. The electrochemical synthesis of H_2O_2 from renewable electricity and naturally abundant educts O_2 and H_2O is a promising pathway compared to the current AO process [7]. There are two possible electrochemical routes for H_2O_2 production, i.e., via cathodic and anodic reactions. The cathodic route is based on the O_2 reduction in an aqueous medium (Eq. (1)) using catalysts based on carbon [26–29], noble metals (Au, Ag [7] and Pd [30]), noble metal alloys (e.g. Pt-Hg [31], Pd-Au [32]) or compounds like PtP_2 [33]. From the perspective of minimizing process costs, non-noble metal-based electrocatalysts such as Ni_3B are more attractive [34]. Many reactor designs, including pressurized-jet microfluidic flow-through reactor, have been developed to enhance O_2 solubility, maximizing reaction efficiency, and reducing energy consumption [35,36]. The anodic formation of H_2O_2 proceeds via two-electron oxidation of water (Eq. (2)) at the anode [7,37]. This anodic route is particularly promising because it can be combined with many cathodic reactions, including the cathodic production of H_2O_2 via oxygen reduction reaction (ORR), hydrogen

* Corresponding author.
E-mail address: luciana.vieira@igb.fraunhofer.de (L. Vieira).

https://doi.org/10.1016/j.apcatb.2021.120848
Received 10 June 2021; Received in revised form 13 October 2021; Accepted 23 October 2021
Available online 29 October 2021

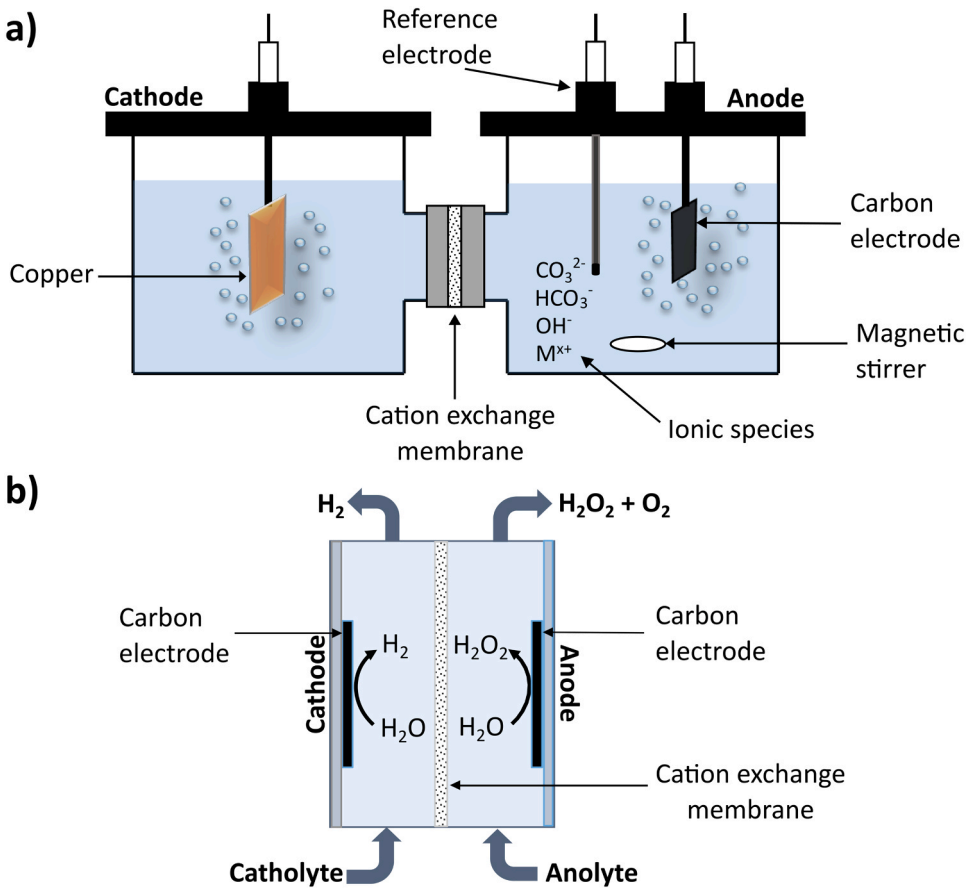

Fig. 1. Schematic representation of the utilized electrochemical cells. (a) H-cell equipped with a 1 cm^2 carbon anode and a 7.5 cm^2 cm copper plate cathode at 6 cm distance. (b) Flow cell with 10 cm^2 carbon electrodes (cathode and anode) at 8 mm electrode distance. 200 mL of the electrolyte solution in a reservoir was used in each flow cell compartment circulating at a rate of 100 mL min^{-1}. Both cells were separated by a Nafion 117 membrane.

evolution reaction (HER), and CO_2 reduction reaction (CO_2RR), thus enabling productive utilization of both half-cell reactions.

$$O_2 + 2H^+ + 2e^- \rightarrow H_2O_2 \; E^0 = 0.67V \text{ vs. RHE} \quad (1)$$

$$2H_2O \rightleftharpoons H_2O_2 + 2H^+ + 2e^- \; E^0 = 1.76V \text{ vs. RHE} \quad (2)$$

Recent research efforts regarding the anodic production of H_2O_2 have focused on catalyst materials and electrode development to enable high selectivity towards H_2O_2. Various metal oxides, including $BiVO_4$, $CaSnO_3$, ZnO, WO_3, SnO_2, and TiO_2, have been reported as active electrocatalysts for the anodic synthesis of H_2O_2 [37–42]. High faradaic efficiencies (up to 80%) have been reported for those systems, albeit only at low current densities (0.1–15 mA cm^{-2}) [37–42] with H_2O_2 production rate up to 5.7 μmol min^{-1} cm^{-2} [38]. Carbon-based materials coated with hydrophobic polymers (PTFE/CFP) have shown exceptional catalytic performance in terms of activity and electrode stability, with an excellent production rate of 23.4 μmol min^{-1} cm^{-2} in 1 mol L^{-1} Na_2CO_3 [43]. Boron-doped diamond (BDD) electrodes have also been reported as remarkable materials for water oxidation to H_2O_2, with outstanding production rates of 19.7 μmol min^{-1} cm^{-2} in 2 mol L^{-1} $KHCO_3$ [44]. Yet, the electrochemical oxidation of water to H_2O_2 depends not only on the choice of the electrode material but also on reaction parameters, particularly the current/potential applied, electrolyte concentration, pH, and H_2O_2 stabilizers [45,46].

The highest H_2O_2 concentration ever achieved by electrochemical methods was 20 wt% H_2O_2 solution via electrochemical O_2 reduction using a solid electrolyte setup [47]. With this exception, the concentration of H_2O_2 produced electrochemically is, in general, relatively low compared to that achievable by the current AO process. Nevertheless, the relatively lower H_2O_2 concentrations achieved electrochemically are already promising for healthcare and environmental applications. Moreover, the electrochemical route would enable the decentralization of H_2O_2 production, requiring only an electrochemical device and electricity [45]. Decentralized electrocatalytic H_2O_2 production could be an enabling technology for local disinfectant production in the concept of future hospitals [48] as well as in remote places in the fight against COVID-19, SARS-CoV-2, MERS [49,50], Ebola [49,51], and Zika [49] viruses. Furthermore, an integrated solar-electricity-driven water treatment process would enable removing recalcitrant chemicals [52–54] and bacteria [54,55].

This study identifies and applies optimized electrolyte conditions for the anodic oxidation of water to H_2O_2. These optimized operating conditions enabled the maximization of the activity, selectivity, efficiency, and stability of the electrochemical process, aiming high H_2O_2 concentration. We have used unmodified commercial carbon materials as electrocatalysts due to their high surface area, relatively high conductivity, and chemical stability in alkaline electrolytes. These carbon materials are easy to use and have considerably low costs. Firstly, different carbon materials were screened for their catalytic activity in a two-compartment stationary H-cell. Carbon cloth, carbon fiber paper, carbon felt, glassy carbon, and carbon gas diffusion layer were used as electrode materials. Outperforming material was further investigated in a 10 cm^2 flow cell, offering more relevant operational conditions in the light of potential future applications and scale-up. The impact of current density (*j*) and potential variation, pH control, electrolyte concentration, and the presence of a chemical stabilizer has been analyzed and the most suitable reaction parameters for the anodic production of H_2O_2 in high concentrations have been identified. Additionally, the impact of HCO_3^-

and CO_3^{2-} ions' activity in the electrolyte on the electrochemical H_2O_2 production was examined, indicating clearly the importance of CO_3^{2-} ions for the anodic H_2O_2 production.

2. Material and methods

2.1. Characterization

The surface morphology of all the different carbon materials was examined by a scanning electron microscope (SEM Carl Zeiss DSM 940A Oberkochen, Germany) at 20 kV and 6 mm working distance. The electrode materials were placed onto a carbon tape on top of an alumina plate sample holder. The thickness of each carbon material was measured with ImageJ from at least 10 different areas of an SEM image.

2.2. Electrochemical measurements

Electrochemical measurements were performed at room temperature and atmospheric pressure using an Autolab PGSTAT128N potentiostat/galvanostat coupled with a 10 A booster. Screening experiments were performed in a two-compartment H-Cell (Fig. 1a) with a three-electrode configuration separated by an ion-exchange membrane (Nafion 117, Ion Power, Germany). Carbon cloth (W1S1005), carbon fiber paper (TP-060), gas diffusion layer (Freudenberg, H23C9), all from Quintech, Germany, glassy carbon rod (Metrohm, 61247000) and carbon felt (Alfa Aesar, 43200) were used as electrodes without further treatment. Carbon samples with a geometric area of 1 cm^2 were used as anode, 7.5 cm^2 copper plate as cathode, and Ag/AgCl in 3.5 mol L^{-1} KCl (eDAQ) as a reference electrode. 25 mL of 2 mol L^{-1} potassium hydrogen carbonate ($KHCO_3$, Sigma Aldrich, 99.5%) was chosen as standard electrolyte [41] and was freshly prepared prior to each experiment. Linear sweep voltammetry (LSV) at 10 mV s^{-1} and chronopotentiometry at 50 mA cm^{-2} (related to the geometric area of the anode) were measured for each carbon material. The cell potential was recorded with a voltammeter. The pH of the electrolyte was regulated with the addition of potassium hydroxide (KOH, Carl Roth) salt or CO_2 bubbling. The electrolyte conductivity was measured with a conductometer (VWR pHenomenal® CO 3100 H) and the pH with a pH-meter (VWR pH 3210). Potassium carbonate (K_2CO_3, ≥99%, Carl Roth) and sodium metasilicate (Na_2SiO_3, Sigma Aldrich) were used as received.

After the material screening, the best performing electrode was evaluated by chronoamperometry with multiple potential steps. The concentration of H_2O_2 was measured at each step potential, in intervals of 0.2 V from +1.2 V to +2 V vs. Ag/AgCl, with 10 min at each step. The corresponding current densities were calculated using the geometric area of the electrode.

Flow cell experiments were carried out in a Microflow cell (Electrocell, Denmark) (Fig. 1b) with 10 cm^2 (3 cm × 3.5 cm) electrodes separated by a Nafion 117 cation exchange membrane (CEM). 200 mL of the electrolyte solution was circulated in each compartment with a 100 mL min^{-1} flow controlled by a flow pump (Watson-Marlow) in a flow range varying from 2 to 120 mL min^{-1}.

2.3. H_2O_2 analysis

The analytic quantification of H_2O_2 in an electrochemical system can be influenced by the type of electrolyte, pH, and other interfering species generated at the electrode [56]. Therefore we used three methods to detect H_2O_2: an enzymatic assay, detection strips, and $KMnO_4$ titration.

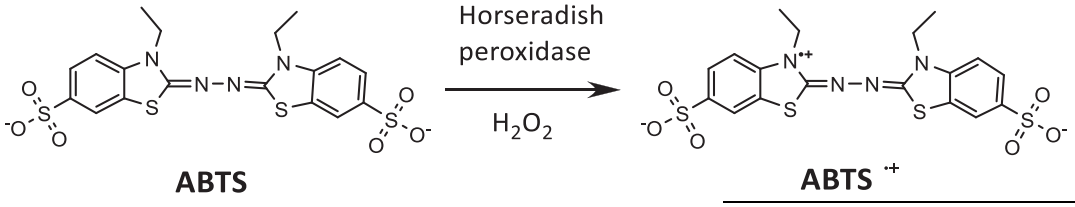

(3)

The enzymatic assay is based on the one-electron oxidation of ABTS ABTS (2,2′-azino-bis(3-ethylbenzothiazoline-6-sulfonic acid), Sigma Aldrich) by H_2O_2 into the corresponding radical cation, $ABTS^{+\bullet}$. This reaction is catalyzed by the enzyme horseradish peroxidase (HRP, Sigma Aldrich) [57,58] (Eq. (3)).

For this enzymatic method, 2 mmol L^{-1} ABTS (in 0.1 mol L^{-1} potassium phosphate buffer, KPi, pH 5.0) and 5.0 mg L^{-1} of horseradish peroxidase (HRP) were freshly prepared before use. A standard cuvette for the photometric investigation was prepared with 1 mL ABTS solution, 0.1 mL of the HRP enzyme, and 0.1 mL of the sample (H_2O_2 in 2 mol L^{-1} $KHCO_3$ solution). The solution was mixed well and kept for 10 min at room temperature. The progression of this enzymatic reaction is accompanied by a color change in the solution from colorless to green, depending on the concentration of H_2O_2. Thereafter, the absorbance of the solution was measured at 405 nm in a Shimadzu UV-1800 spectrophotometer. The molar extinction coefficient (ε_{405nm}) of oxidized ABTS is 36,800 M^{-1} cm^{-1}. The calibration curve is shown in Supporting Information, Fig. S1a.

For the detection with strips, the color intensity of the strip is measured with a strip reader (Quantofix Relax, Macherey-Nagel) [39,44]. As for the titration with $KMnO_4$, a 100 mL electrolyte sample was acidified with 5 mL (1:5) sulfuric acid solution and titrated with 0.02 mol L^{-1} standardized $KMnO_4$ solution as reported in the literature [44,56,59].

All three detection techniques yield comparable results for the standard H_2O_2 solutions. A comparison for all three methods is shown in Supporting Information, Fig. S1b. In all the experiments herein shown, we determined the H_2O_2 concentration with the detection strip and confirmed it with the ABTS assay.

The faradaic efficiency (FE) of the produced H_2O_2 was calculated by the following equation (Eq. (4)):

$$FE(\%) = \frac{H_2O_2 \text{ detected}(mol) \times \text{no. of electrons} \times \text{Faraday constant (C mol}^{-1})}{\text{total charge passed (C)}} \times 100 \quad (4)$$

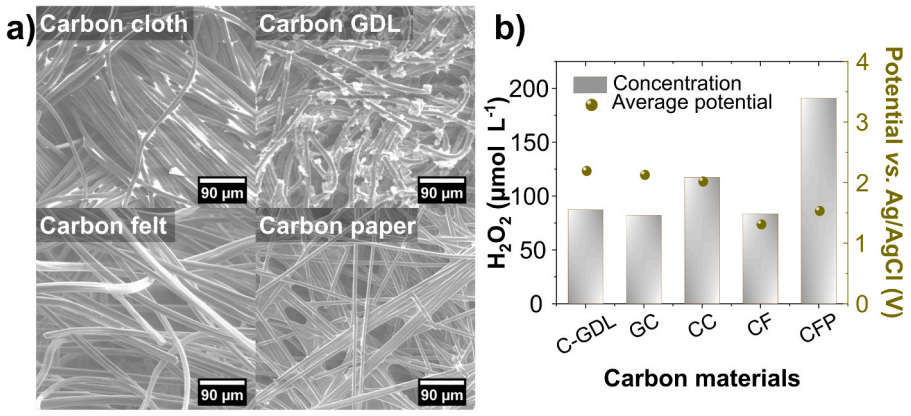

Fig. 2. Selection of carbon material for H_2O_2 synthesis. (a) SEM images of carbon cloth (CC), carbon gas diffusion layer (C-GDL), carbon felt (CF), and carbon fiber paper (CFP) used in this study. (b) H_2O_2 concentration in the anolyte and average electrode potential (vs. Ag/AgCl) during electrolysis using different carbon materials at 50 mA cm^{-2} for 10 min at room temperature.

Table 1
Performance of different carbon materials for H_2O_2 production. Anodic H_2O_2 production with different carbon materials as electrode after 10 min galvanostatic polarization at 50 mA cm^{-2}. The potential corresponds to the average electrode potential during electrolysis.

Carbon material	H_2O_2 concentration	Highest H_2O_2 production rate	Maximum H_2O_2 FE	Potential
	µmol L^{-1}	µmol min^{-1} cm^{-2}	%	V *vs.* Ag/AgCl
Carbon fiber paper (CFP)	190.9	0.48	3.1	1.5
Carbon cloth (CC)	117.2	0.29	1.9	2.0
Gas diffusion layer (C-GDL)	87.3	0.22	1.4	2.2
Carbon felt (CF)	83.5	0.21	1.3	1.3
Glassy carbon (GC)	82.0	0.21	1.3	2.1

where the number of electrons is 2 for water oxidation to H_2O_2, and the Faraday constant is 96485 C mol^{-1}.

The production rate of the H_2O_2 produced is given by Eq. (5):

$$\text{Production rate}(\mu mol\ min^{-1}cm^{-2}) = \frac{H_2O_2\ \text{detected}(\mu mol)}{\text{time}(min) \times \text{area of the electrode}(cm^2)} \quad (5)$$

2.4. Calculation of the ionic activities for HCO_3^- and CO_3^{2-}

To address the question of how the bicarbonate (HCO_3^-)/ carbonate (CO_3^{2-}) species affect the productivity of H_2O_2, a speciation analysis was carried out, taking into account the equilibrium of ions in the solution according to Eqs. (6) and (7). Depending on the pH of the solution, different carbonate species (H_2CO_3, HCO_3^-, and CO_3^{2-}) as well as H_2O_2 (as H_2O_2 and HOO^-) can be present in the solutions (Supporting Information, Fig. S2) [37,60,61].

$$H_2CO_3 \rightleftharpoons HCO_3^- + H^+ \ (pK_{a,1} = 3.7) \quad (6)$$

$$HCO_3^- \rightleftharpoons CO_3^{2-} + H^+ \ (pK_{a,2} = 10.3) \quad (7)$$

The molar fraction (α) of each species was calculated based on Eqs. (9) and (10). Since the experiments were carried out in highly concentrated electrolytes which deviate from the ideal behavior of diluted electrolytes, the ion activities ($a_{HCO_3^-}$ and $a_{CO_3^{2-}}$) were calculated as shown in Eqs. (11) and (12) using the activity coefficient ($f_\pm$) shown in Eq. (13), where z_i is the charge of the ion, A is Debye-Hückel parameter (0.51 $kg^{½}$ $mol^{-½}$, for water at 25 °C), and B is a temperature-dependent parameter. Based on the pH change and carbonate equilibria, we calculated the activity of HCO_3^- ($a(HCO_3^-)$) and CO_3^{2-} ($a(CO_3^{2-})$) ions dependent on the pH of the electrolyte during electrolysis for each concentration (c) of $KHCO_3$.

$$K_{a,i} = 10^{-pK_{a,i}} \quad (8)$$

$$\alpha_{HCO_3^-} = \frac{K_{a,1}.[H^+]}{[H^+]^2 + K_{a,1}.[H^+] + K_{a,1}.K_{a,2}} \quad (9)$$

$$\alpha_{CO_3^{2-}} = \frac{K_{a,1}.K_{a,2}}{[H^+]^2 + K_{a,1}.[H^+] + K_{a,1} * K_{a,2}} \quad (10)$$

$$a_{HCO_3^-} = \alpha_{HCO_3^-}.c_{KHCO_3}.f_\pm \quad (11)$$

$$a_{CO_3^{2-}} = \alpha_{CO_3^{2-}}.c_{KHCO_3}.f_\pm \quad (12)$$

$$log f_\pm = -\frac{A.Z_i^2 \bullet \sqrt{j}}{1 + B.a_i \bullet \sqrt{j}} \quad (13)$$

3. Result and discussion

3.1. Selection of carbon material

Commercial carbon materials were evaluated for the anodic synthesis of H_2O_2 in a two-compartment H-cell. The materials comprise carbon gas diffusion layer (C-GDL), glassy carbon (GC), carbon cloth (CC), carbon felt (CF), and carbon fiber paper (CFP). SEM images of each carbon electrode are depicted in Fig. 2a. All materials except GC were fibrous. CFP and CF were highly porous, whereas CC and C-GDL were more compact. The fibers' average thickness for C-GDL, CC, CF, and CFP was 11.0, 8.7, 15.5, and 7.9 µm, respectively.

The current densities of different materials upon anodic polarization were evaluated in a first screening step by LSV (Supporting Information, Fig. S3a). The lowest onset potential was observed for CF (1.16 V vs. Ag/AgCl) followed by CFP. Exceptionally high current densities of 399 and 177 mA cm^{-2} at 2 V vs. Ag/AgCl were obtained with CF and CFP electrodes, respectively, indicating high water oxidation affinity (to O_2 and/or H_2O_2) for these two materials.

In a second step, the H_2O_2 production was measured quantitatively after 10 min of galvanostatic polarization at 50 mA cm^{-2}, which

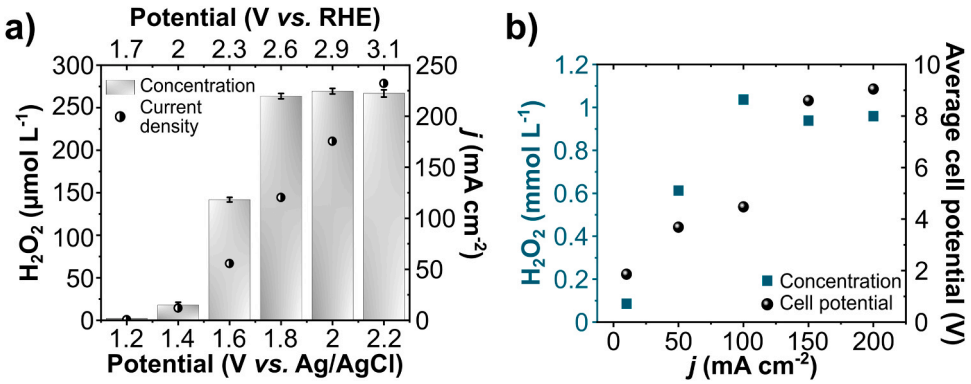

Fig. 3. Impact of operating potential and current density. (a) H_2O_2 concentration and current density at different applied potentials in 2 mol L^{-1} $KHCO_3$ in an H-Cell. (b) Final H_2O_2 concentration and average cell potential after 150 min of electrolysis at different applied current densities in a flow cell using 2 mol L^{-1} $KHCO_3$ at 100 mL min^{-1} flow rate.

provided a constant 30 C charge for each electrode material. Among the investigated carbon materials, CFP revealed the highest selectivity and FE towards H_2O_2, with a FE of 3.1% and a maximum production rate of 0.48 μmol min^{-1} cm^{-2}, followed by CC, C-GDL, CF, and GC as shown in Table 1 and Fig. 2b. Compared to the other carbon materials, CF and CFP showed the lowest electrode potential during the galvanostatic experiments, with 1.3 and 1.5 V vs. Ag/AgCl, respectively. The different electrochemical activity of the carbon materials toward WOR could be caused by the materials difference in electrode structure, the hydrophobicity of the surface, and due to the transport of the reaction products. The lowest activity of GC is likely due to its 2D structure. All carbon materials except GC are fibrous, with a 3D structure. Hence, the electrochemical active area of GC is considerably lower than the other carbon materials. CFP and CF are highly porous, whereas CC and C-GDL are more compact 3D structures, as shown in the SEM images of Fig. 2a. The product transport characteristics in the electrode materials are determined by their porosity, permeability, and hydrophobicity [62]. CC and C-GDL materials are treated with PTFE. One side of CC and C-GDL consists of a microporous layer (MPL) made of carbon and a hydrophobic agent. Earlier reports have suggested an enhanced activity towards H_2O_2 production upon increasing the hydrophobicity [43]. However, we observed a lower electrochemical H_2O_2 production in CC and C-GDL (Table 1 and Fig. 2b). A summary of the technical specification of these carbon materials is shown in the Supporting Information, Table S2**.** Due to its low onset potential, higher H_2O_2 selectivity, production rate, and consequently the highest achieved H_2O_2 concentration, CFP was chosen for further investigations.

It should be noted that the H_2O_2 selectivity and production rate observed in these initial experiments on CFP are relatively low compared to values reported in the literature using PTFE/CFP in 1 mol L^{-1} Na_2CO_3 [43]. Nevertheless, these initial measurements have been conducted under operational conditions that had not been

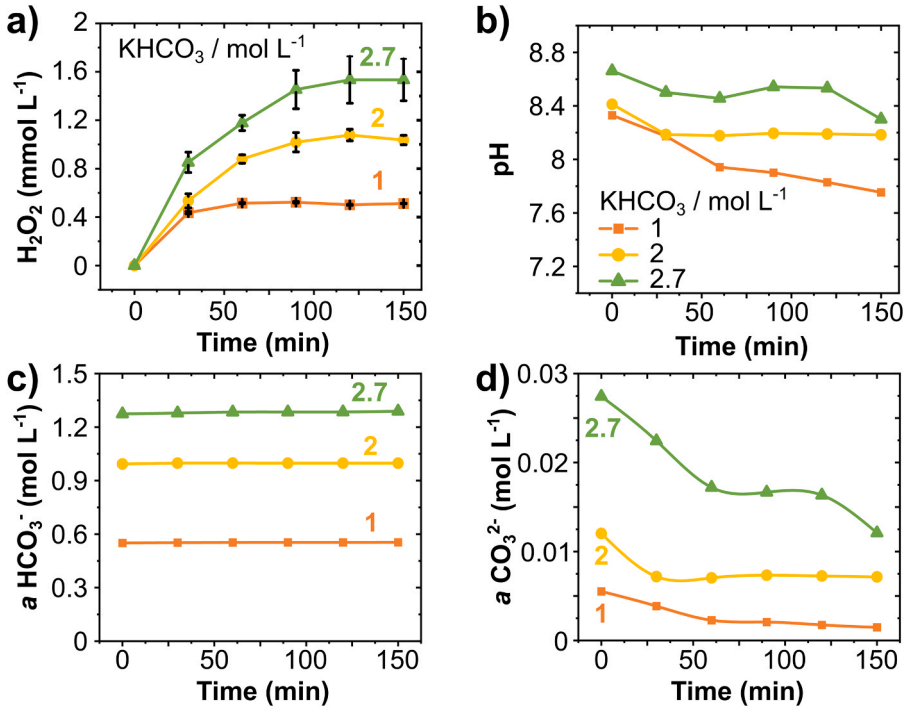

Fig. 4. Anodic H_2O_2 production in $KHCO_3$ electrolyte with different concentrations. (a) H_2O_2 production over time, (b) pH variation, (c) HCO_3^- activity, and (d) CO_3^{2-} activity in the anolyte circulated with 1, 2 and 2.7 mol L^{-1} $KHCO_3$ ■ ● ▲. Experiment conditions: flow cell at 100 mA cm^{-2} for 150 min and 200 mL anolyte circulated at 100 mL min^{-1}.

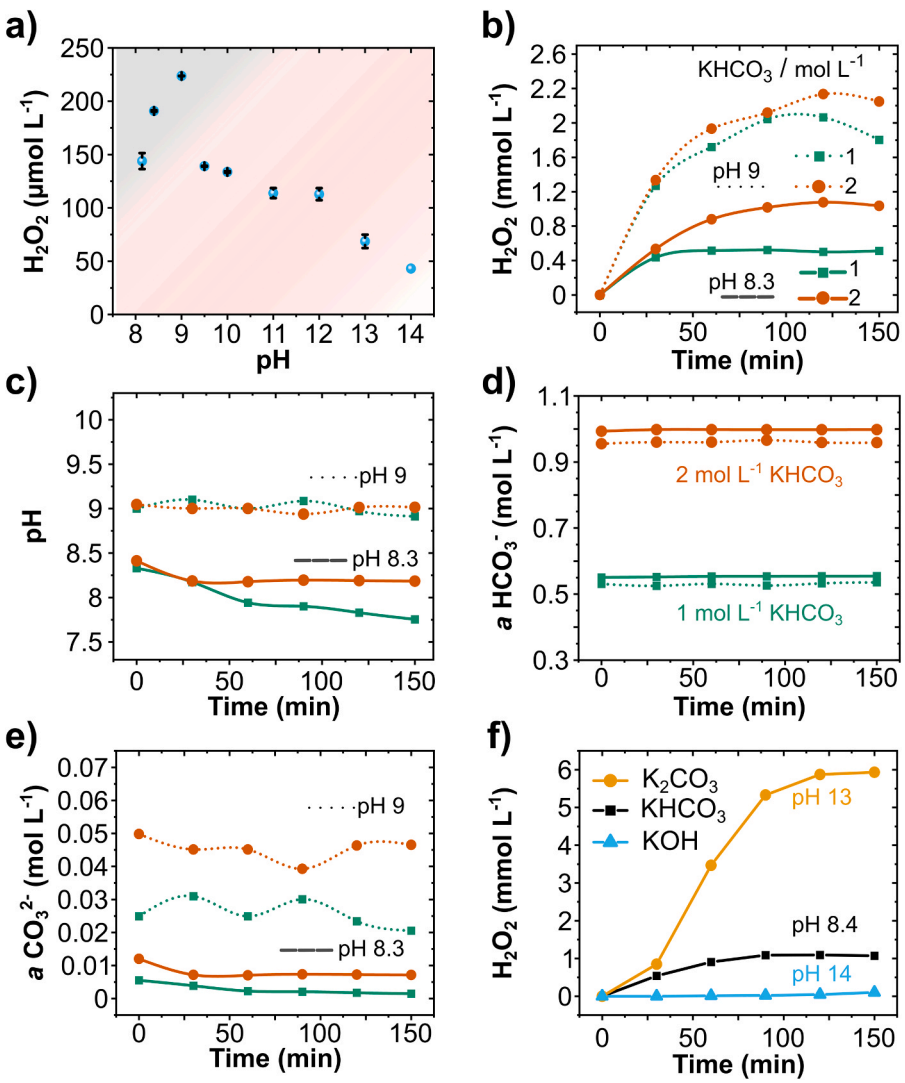

Fig. 5. Study of the anodic H_2O_2 generation in 1 mol L^{-1} and 2 mol L^{-1} $KHCO_3$ electrolytes at different pH. (a) anodic H_2O_2 production with pH variation in 2 mol L^{-1} $KHCO_3$ at 50 mA cm^{-2} for 10 min in an H-cell. (b) H_2O_2 production, (c) pH change, and (d) $a(HCO_3^-)$ and (e) $a(CO_3^{2-})$ in the anolyte circulated with (■) 1 mol L^{-1} or (●) 2 mol L^{-1} $KHCO_3$. Solid lines correspond to non-regulated pH experiments. Dotted lines correspond to experiments with pH control at pH 9. (f) H_2O_2 production in ■ 2 mol L^{-1} $KHCO_3$, ● K_2CO_3, and ▲ KOH. 30 mmol L^{-1} of Na_2SiO_3 was added to 2 mol L^{-1} K_2CO_3 and to 2 mol L^{-1} KOH as a stabilizer to prevent decomposition of H_2O_2 at high pH. Experimental conditions for (b–e): flow cell at 100 mA cm^{-2} for 150 min with 200 mL electrolyte at 100 mL min^{-1}.

optimized. The following sessions will show how the optimization of reaction parameters is crucial to enhance the final anodic H_2O_2 production on CFP electrodes.

3.2. Effect of potential and current density

The anodic H_2O_2 production upon variation of potential and current density was evaluated on CFP electrodes. Potentiostatic experiments varying the potential positively stepwise from +1.2 V to +2.2 V vs. Ag/AgCl in an H-cell (Fig. 3a) showed the highest H_2O_2 concentration of 270 μmol L^{-1} at +2.0 V vs. Ag/AgCl with a current density (j) of ~175 mA cm^{-2}. The maximum production rate at this potential (+2.0 V) was 0.67 μmol min^{-1} cm^{-2} after 10 min (the potential screening data is shown in Supporting Information, Table S1 and Fig. S4a). At +1.8, +2.0, and +2.2 V vs. Ag/AgCl, the H_2O_2 formation rate stayed constant at 0.67 μmol min^{-1} cm^{-2}, despite the increase in current density from 120 to 232 mA cm^{-2} at the same potential range, indicating most of the current is consumed for O_2 evolution at more positive potentials. Further study at higher potentials led to an increase in the current density, though considerably lower H_2O_2 concentration, indicating a preference for water oxidation to O_2 (Supporting Information, Fig. S4b).

The setup was transferred to a flow cell, where galvanostatic experiments with the current density being raised stepwise from 10 to 200 mA cm^{-2} showed a maximum concentration of H_2O_2 (1.1 mmol L^{-1}) at 100 mA cm^{-2} (Fig. 3b). At 150 mA cm^{-2}, the H_2O_2 concentration had a peak at 120 min (1.2 mmol L^{-1}), decaying to 0.9 mmol L^{-1} after 150 min (H_2O_2 concentration versus time at different current densities is shown in Supporting Information, Fig. S4c). This decay in H_2O_2 concentration indicates the decomposition of the generated H_2O_2 on the electrode surface. The same behavior was observed at 200 mA cm^{-2}. Since the standard potential for H_2O_2 oxidation (0.67 V vs. RHE, Eq. (15)) is considerably lower than the standard potential for water oxidation to H_2O_2 (1.76 V vs. RHE, Eq. (2)), the electrogenerated H_2O_2 can decompose to O_2 in the vicinity of the electrified electrode surface. Moreover, H_2O_2 is chemically unstable and can self-decompose to O_2. An experiment of chemical stability for electrogenerated H_2O_2 showed a decay of 19% H_2O_2 during 2.5 h at an open circuit (Supporting Information, Fig. S5). Thus, a combined effect of self-and electro-decomposition of H_2O_2 can lead to a limitation of the H_2O_2 concentration to a level where formation and decomposition of H_2O_2 occur at the same rate [63]. Hence, at higher current densities (150 and 200 mA cm^{-2}), a combination of water oxidation to O_2 and H_2O_2 decomposition (Eqs. (14) and (15)) accounts for the lower H_2O_2 concentration.

$$H_2O \rightleftharpoons ½\ O_2 + 2H^+ + 2e^-\ E^0 = 1.23\ \text{V vs. RHE} \quad (14)$$

$$H_2O_2 \rightleftharpoons O_2 + 2H^+ + 2e^-\ E^0 = 0.67\ \text{V vs. RHE} \quad (15)$$

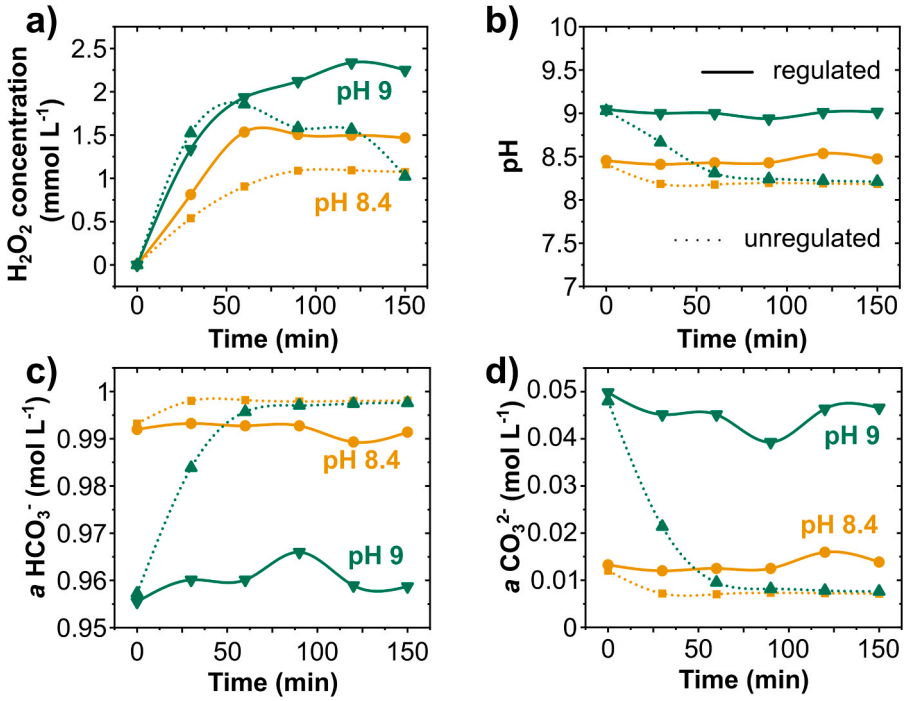

Fig. 6. Anodic H_2O_2 generation in 2 mol L^{-1} $KHCO_3$ electrolyte at different pH. (a) H_2O_2 concentration (b) pH change, (c) $a(HCO_3^-)$ and (d) $a(CO_3^{2-})$ in the anolyte in 2 mol L^{-1} $KHCO_3$ at (● , ■) pH 8.4, and (▼ , ▲) pH 9. Solid lines correspond to experiments with pH regulation during electrolysis. Dotted lines correspond to experiments without pH regulation. Experiment conditions: Flow cell at 100 mA cm^{-2} with 200 mL anolyte at a flow rate of 100 mL min^{-1}.

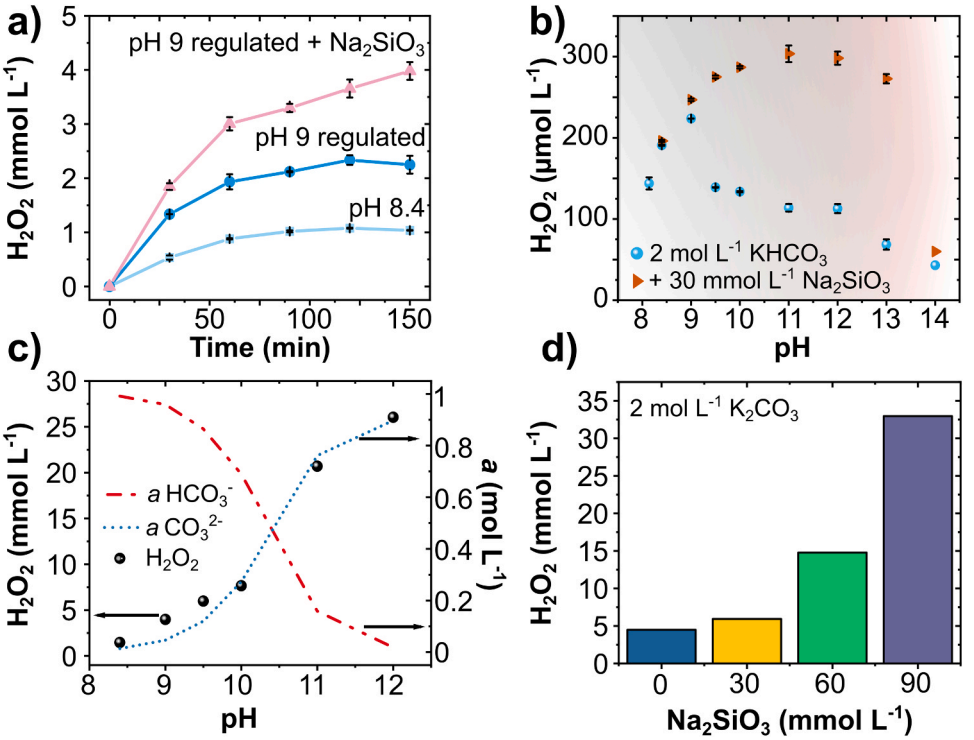

Fig. 7. Effect of Na_2SiO_3 stabilizer on H_2O_2 generation. (a) Anodic H_2O_2 concentration in 2 mol L^{-1} $KHCO_3$ electrolyte at (■) pH 8.4, (●) controlled pH 9, and (▲) at controlled pH 9 with 30 mmol L^{-1} of Na_2SiO_3 as a stabilizer after 150 min at 100 mA cm^{-2} in a flow cell. (b) Anodic H_2O_2 production with pH variation in 2 mol L^{-1} $KHCO_3$ with and without 30 mmol L^{-1} Na_2SiO_3 at 50 mA cm^{-2} for 10 min in an H-cell. (c) H_2O_2 concentration, $a(HCO_3^-)$ and $a(CO_3^{2-})$ in the anolyte at different pH in 2 mol L^{-1} $KHCO_3$ after 150 min of electrolysis at 100 mA cm^{-2} in a flow cell. Up to pH 11, the stabilizer concentration used was 30 mmol L^{-1}. At pH 12, the stabilizer concentration was 90 mmol L^{-1}. (d) H_2O_2 production in 2 mol L^{-1} K_2CO_3 (pH 12.6) with different stabilizer concentrations after 150 min of electrolysis at 100 mA cm^{-2} in a flow cell.

Table 2
Summary of the electrolyte optimization for anodic H_2O_2 production on carbon fiber paper. Experimental conditions: 100 mA cm^{-2} for 150 min, carbon fiber paper anode, and 100 mL min^{-1} electrolyte flow rate. All experiments in this table were carried out with pH control during electrolysis.

Electrolyte	pH	Conductivity mS cm^{-1}	a (HCO_3^-) mol L^{-1}	a (CO_3^{2-}) mol L^{-1}	[Na_2SiO_3] mmol L^{-1}	[H_2O_2] mmol L^{-1}
2 mol L^{-1} $KHCO_3$	8.4	119.4	0.99	0.01	0	1.47
	9.0	123.5	0.96	0.05	0	2.25
	9.0	123.5	0.96	0.05	30	3.98
	9.5	139.2	0.86	0.12	30	5.98
	10.0	152.5	0.69	0.27	30	7.66
	11.0	166.3	0.16	0.76	30	20.70
	12.0	169.4	0.02	0.90	90	**26.04**
2 mol L^{-1} K_2CO_3	12.6	208.0	–	–	0	4.48
		211.0	–	–	30	5.93
		210.0	–	–	60	14.77
		210.0	–	–	90	**32.96**

At current densities higher than 100 mA cm^{-2}, a visual color change was observed in the electrolyte, which turned brown from colorless (Supporting Information, Fig. S6). The oxidation of the carbon surface caused erosion of the electrode, and graphitic carbon particles were exfoliated in the electrolyte [64]. SEM images of the carbon electrodes before and after 150 min of electrolysis at 200 mA cm^{-2} revealed a damaged electrode surface (Supporting Information, Fig. S6). The fiber thickness decreased from 7.9 μm to 3.5 μm, indicating electrode degradation.

The highest H_2O_2 concentration and the lowest cell potential were obtained at 100 mA cm^{-2}, thus this current density was applied for all following electrolyte optimization experiments. To examine electrode stability, cycles of 2.5 h at 100 mA cm^{-2} in 2 mol L^{-1} $KHCO_3$ were performed, in which the electrolyte was changed at every cycle of 2.5 h (Supporting Information, Fig. S7, and S8). Interestingly, upon changing the electrolyte, the H_2O_2 concentration quickly reached a similar concentration as the previous cycle (between 0.6 and 1 mmol L^{-1}), indicating that the maximum H_2O_2 concentration is limited by the electrochemical H_2O_2 decomposition. Moreover, the cell potential was rather constant throughout the cycles. Hence, the CFP electrodes are stable for 7 cycles at 100 mA cm^{-2} (17.5 h). After this time, carbon particles were observed in the anolyte reservoir, indicating oxidation and mechanical disintegration of the electrode.

3.3. Effect of electrolyte concentration

The anodic oxidation of water to H_2O_2 was evaluated in $KHCO_3$ electrolyte with concentrations of 1.0, 2.0, and 2.7 mol L^{-1}. The latter corresponds to a saturated $KHCO_3$ solution at room temperature, as the maximum solubility of $KHCO_3$ in water is 23 g/100 mL (2.3 mol L^{-1}) at 20 °C [65]. LSV of CFP electrodes in these three electrolytes showed considerably higher current densities in more concentrated $KHCO_3$ solutions, indicating that HCO_3^- accelerates water oxidation (LSVs shown in Supporting Information, Fig. S9). Flow cell experiments at 100 mA cm^{-2} showed a three-fold increase in H_2O_2 production upon raising the bicarbonate concentration from 1.0 to 2.7 mol L^{-1} $KHCO_3$: from 0.5 to 1.5 mmol L^{-1} H_2O_2 after 150 min (Fig. 4a). The production rate rises from 0.29 to 0.56 μmol min^{-1} cm^{-2} after 30 min (peak of production rate, see Supporting Information, Fig. S10a, b). Hydrogen carbonate ions (HCO_3^-) have been described as a stabilizing agent and accounted for enhancing the water oxidation to H_2O_2 [32,37,41,44]. The described mechanism for enhancing H_2O_2 production in bicarbonate electrolytes involves the generation of peroxomonocarbonate (HCO_4^-) species at the anode through HCO_3^- oxidation (Eq. (16)). Subsequently, peroxocarbonate species decompose hydrolytically into H_2O_2 and bicarbonate ions, as given in Eq. (17) [37,43,46].

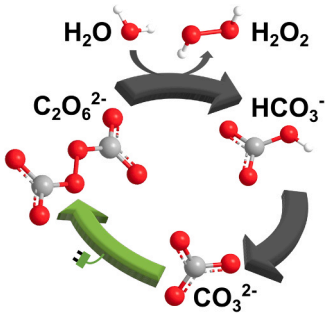

Fig. 8. Suggested mechanism for anodic H_2O_2 production in bicarbonate electrolytes. Bicarbonate ions (HCO_3^-) are deprotonated to carbonate (CO_3^{2-}) in alkaline electrolytes. CO_3^{2-} can be anodically oxidized to peroxodicarbonate ($C_2O_6^{2-}$) species. $C_2O_6^{2-}$ decomposes into HCO_3^- and hydrogen peroxide (H_2O_2), closing the cycle with a higher H_2O_2 concentration.

$$HCO_3^- + H_2O \rightleftharpoons HCO_4^- + 2H^+ + 2e^- \quad E^0 = 1.80 \text{ V vs. RHE} \tag{16}$$

$$HCO_4^- + H_2O \rightarrow H_2O_2 + HCO_3^- \tag{17}$$

The anodically produced H_2O_2 reaches a concentration plateau within 90 min of electrolysis (Fig. 4a). At more concentrated $KHCO_3$ electrolytes, the plateau rises to a higher H_2O_2 concentration range. These limiting values of the H_2O_2 concentration can be due to concurrent O_2 formation and electrodecomposition of H_2O_2 [44,66]. The higher rate of H_2O_2 generation increases the rate of H_2O_2 decomposition until a steady-state is reached. An experiment adding 0.9 mmol L^{-1} H_2O_2 as initial concentration led to a similar concentration plateau where no H_2O_2 was added (Supporting Information, Fig. S11), suggesting a dynamic steady-state with a limiting H_2O_2 concentration. Hence, the main challenge is to raise the plateau to the highest possible H_2O_2 concentration.

The pH of the $KHCO_3$ anolyte was constantly monitored and all electrolyte concentrations showed a pH decline during electrolysis (Fig. 4b). The initial pH in 1, 2, and 2.7 mol L^{-1} $KHCO_3$ are 8.3, 8.4, and 8.7, respectively. After 150 min, it decreased to 7.7, 8.1, and 8.3. This slight anolyte acidification is caused by the electro-oxidation of water (Eqs. (2) and (14)).

Based on pH variation during electrolysis, we calculated the variation of ionic activity for HCO_3^- ($a(HCO_3^-)$) and CO_3^{2-} ($a(CO_3^{2-})$) species in the electrolyte (Fig. 4c, d). The equilibrium between HCO_3^- and CO_3^{2-} ions is pH-dependent, and at a pH range from 8 to 9, the activity of HCO_3^- ions is higher than CO_3^{2-} (Supporting Information, Fig. S2). $a(HCO_3^-)$ and $a(CO_3^{2-})$ increase accordingly with electrolyte concentration (Fig. 4c, d). In this pH range, $a(CO_3^{2-})$ is two orders of magnitude smaller than that of $a(HCO_3^-)$ and decreases during electrolysis, whereas the activity of $a(HCO_3^-)$ ions appears to be constant at each concentration (Fig. 4c, d). Varying the concentration of the electrolyte leads to a change in the pH, ionic activity for HCO_3^- and CO_3^{2-} ions in the electrolyte. Experiments with and without the addition of

Table 3
A comparison of the reported work on water oxidation to H_2O_2 with our present study.

Electrode	Cell type	Electrolyte	pH	$[H_2O_2]_{max}$	Conditions[a]					Production rate	Peak FE	Ref.
				mmol L^{-1}	*j*/E	t	EA	VA	S	*μmol* min^{-1} cm^{-2}	%	
PTFE/CFP	H-Cell	1 M Na_2CO_3	12	3	100	420	0.36	25	~30	23.4	66	[43]
BDD/Nb			11.9	–	39.8	10	1.13	8.5	–	3.93	31.7	[80]
BDD/Ti		2 M $KHCO_3$	8	~ 16	120	5	7.4	25	–	~ 8	28	[44]
BDD/Ti			8	29	295	5	7.4	25	–	19.7	~ 22	[44]
$CaSnO_3$/FTO	Undivided		8.3	–	3.2 V	10	–	30	–	~ 4.6	76	[39]
$CaSnO_3$/FTO			8.3	~ 0.9	2.2 V	720	–	30	–	–	–	[39]
$BiVO_4$/FTO		1 M $NaHCO_3$	8.3	–	3.1 V	–	1	20	–	5.7	70	[38]
CFP	Flow-Cell	2 M $KHCO_3$	8.4	1.47	100	150	10	200		0.5	1.7	This work
CFP			12	26	100	150	10	200	90	4	13.1	
CFP		2 M K_2CO_3	12.6	**33**	100	150	10	200	90	4.5	14.3	

[a] j: Current density (mA cm^{-2}), E: Potential applied (V vs. RHE), t: Time (min), EA: Electrode area (cm^2), VA: Volume of anolyte (mL), S: Stabilizer concentration (mmol L^{-1} Na_2SiO_3).

$KHCO_3$ during the electrolysis reveals that increasing the $KHCO_3$ concentration results in an increase of (i) H_2O_2 production, (ii) pH, (iii) conductivity, and (iv) activity of HCO_3^- and CO_3^{2-} ions (Supporting Information, Fig. S12a–e). It is possible that the higher anodic H_2O_2 production results from a combined effect of higher pH and ratio of the activity of HCO_3^- and CO_3^{2-} ions in the electrolyte. Thus, we have investigated these two parameters in more detail, discussed in the following sections.

3.4. Effect of pH

Experiments described in the previous section showed that a higher concentration of HCO_3^- ions boost H_2O_2 production. However, in the electrolyte, the distribution of the HCO_3^- and CO_3^{2-} ion is pH-dependent [37]. Upon carrying out long-term electrosynthesis, a significant pH shift was observed towards a more acidic electrolyte, which leads to a change of HCO_3^-/ CO_3^{2-} ratio in the solution. Earlier studies reporting H_2O oxidation to H_2O_2 upon pH variation between 7 and 12.5 in 0.5 mol L^{-1} $KHCO_3$ showed lower H_2O_2 production at higher pH [37]. The authors attributed the lower H_2O_2 production in more alkaline electrolytes to the higher concentration of CO_3^{2-} ions.

In this work, we have investigated in detail the effect of pH variation on the anodic oxidation of water by adjusting the pH of a 2 mol L^{-1} $KHCO_3$ anolyte between 8 and 14. The pH was varied through CO_2 bubbling or KOH addition. LSVs in 2 mol L^{-1} $KHCO_3$ at pH 8.4, 9, 9.5, and 10 (Supporting Information, Fig. S13) revealed lower onset potential and higher current densities upon increasing the pH, indicating not only the increase in conductivity but also higher electrolyte reactivity in more alkaline medium.

Quantitative measurements in anolytes with pH from 8.14 to 14 were performed in an H-cell at a constant current of 50 mA cm^{-2} (Fig. 5a). The initial pH of a typical 2 mol L^{-1} $KHCO_3$ solution is 8.4. At this initial pH, 191 μmol L^{-1} H_2O_2 is formed anodically after 10 min. Decreasing the pH to 8.12 causes a decline in final H_2O_2 concentration to 144 μmol L^{-1}. Increasing the pH to 9 leads to a H_2O_2 concentration of 225 μmol L^{-1}. However, raising pH beyond 9 causes a decline in H_2O_2 production, caused by an increasing rate of decomposition of H_2O_2 in alkaline pH. Thus, at these conditions of electrolyte concentration and current density, the maximum H_2O_2 concentration was obtained at pH 9.

A set of flow cell experiments at 100 mA cm^{-2} was carried out in 1 mol L^{-1} and 2 mol L^{-1} $KHCO_3$, both at pH 8.3 and 9. Upon increasing the pH from 8.3 to 9, a fourfold increase in H_2O_2 production was achieved in 1 mol L^{-1} $KHCO_3$ (from 0.5 to 2 mmol L^{-1} H_2O_2) and a twofold in 2 mol L^{-1} $KHCO_3$ (from 1.1 to 2.4 mmol L^{-1} H_2O_2) (Fig. 5b). The pH was constantly monitored and regulated with KOH addition upon pH decrease (Fig. 5c). It is important to remark that the amount of KOH added is negligible compared to the $KHCO_3$ concentration; hence it does not impact the $a(HCO_3^-)$ or $a(CO_3^{2-})$. Furthermore, we observed that a slightly basic regime (at pH 9) enhances the electrochemical H_2O_2 production. Nevertheless, increasing the bicarbonate concentration from 1 to 2 mol L^{-1} $KHCO_3$ at pH 9 does not significantly improve the H_2O_2 final concentration. This suggests that it is not the HCO_3^- concentration but the pH regime or the CO_3^{2-} concentration being affected by the pH regime that enhances the H_2O_2 production.

Under basic conditions, HCO_3^- ions dissociate into proton (H^+) and carbonate ions (CO_3^{2-}) (Eq. (7)) [37,60]. Raising the pH from 8.3 to 8.4–9 in 1 and 2 mol L^{-1} $KHCO_3$ solutions showed that $a(HCO_3^-)$ is most affected by the electrolyte concentration, whereas $a(CO_3^{2-})$ varies accordingly with the pH change (Fig. 5d, e), due to the dissociation of bicarbonate in alkaline medium. In 1 mol L^{-1} $KHCO_3$, the average a (HCO_3^-) ions decreased by 5.5% upon increasing the pH (Fig. 5d), whereas the $a(CO_3^{2-})$ increased 10 times (Fig. 5e), however the absolute changes are the same. A similar behavior of lower $a(HCO_3^-)$ and higher $a(CO_3^{2-})$ is depicted for 2 mol L^{-1} $KHCO_3$ at pH 9. A correlation between the increase in $a(CO_3^{2-})$ and an enhanced H_2O_2 production was also observed, as higher H_2O_2 concentrations were obtained at higher pH.

CO_3^{2-} ions have been previously reported to be unsuitable for the selective oxidation of water to H_2O_2 compared to HCO_3^- ions [37,41]. On the other hand, Xia et al. [43] reported higher anodic H_2O_2 production in 1 mol L^{-1} Na_2CO_3 (pH 10.3) compared to 1 mol L^{-1} $NaHCO_3$ (pH 8.3), suggesting that CO_3^{2-} ion enhances the H_2O_2 production than the HCO_3^- ions. Considering the active role of CO_3^{2-} ions and the tendency of H_2O_2 to undergo base-catalyzed decomposition in alkaline media, we have changed the electrolyte from 2 mol L^{-1} $KHCO_3$ (pH 8.4) to 2 mol L^{-1} K_2CO_3 (pH 13). 30 mmol L^{-1} Na_2SiO_3 was added to the anolyte to inhibit the H_2O_2 decomposition at high pH [67]. Changing the electrolyte caused an increase in the anodic H_2O_2 production, namely from 1.1 mmol L^{-1} H_2O_2 in $KHCO_3$ to 5.9 mmol L^{-1} in the K_2CO_3 electrolyte (Fig. 5f). Keeping the pH high at around 14 and changing the electrolyte to 2 mol L^{-1} KOH + 30 mmol L^{-1} Na_2SiO_3 resulted in negligible production of H_2O_2. Thereby, the active role of carbonate ions, and not of the alkaline pH regime, in promoting water oxidation to H_2O_2 was confirmed.

During electrolysis, the pH of the 2 mol L^{-1} $KHCO_3$ electrolyte decreases due to the constant oxidation of OH^- ions. In a typical experiment, the final pH of the anolyte is 8.2 after 150 min of anodic polarization, irrespective of the initial pH (9 or 8.4, Fig. 6). The final H_2O_2 concentration is also 1 mmol L^{-1} for both experiments. This pH decrease leads to a drop in both: $a(CO_3^{2-})$ and H_2O_2 production (Fig. 6). At pH 9, the peak production of H_2O_2 is achieved after 60 min (1.9 mmol L^{-1} H_2O_2), with a subsequent decline, presumably due to reduced $a(CO_3^{2-})$ (Fig. 6d). Active adjustment of the pH to achieve constant values at 8.4 and 9 throughout the electrolysis enhanced the H_2O_2 production considerably. For instance, pH regulation at 9 promoted an increase in H_2O_2 production after the 60 min peak, reaching 2.2 mmol L^{-1} H_2O_2 after 150 min. This correlation of higher pH, higher $a(CO_3^{2-})$, and higher H_2O_2 production endorses the hypothesis that

higher $a(CO_3^{2-})$ enhances the generation of H_2O_2 by either generating peroxocarbonate species or stabilizing the peroxide and avoiding its further anodic oxidation by forming a percarbonate adduct [68].

3.5. Effect of stabilizer

H_2O_2 is an unstable compound, decomposing to water and molecular oxygen, as shown in Eq. (18).

$$2H_2O_2 \rightarrow O_2 + 2H_2O \quad (18)$$

To slow down the H_2O_2 decomposition, organic stabilizers such as aryl alkyl ketones are used in practice [69]. These stabilizers are redox-active compounds, which can sacrificially oxidize if added to an electrolytic cell. To prevent the anodic degradation of such compounds during H_2O_2 production, we have chosen a non-redox active additive to stabilize H_2O_2, namely sodium metasilicate (Na_2SiO_3) [67]. Previous experiments using 4 mg mL^{-1} Na_2SiO_3 in 1 mol L^{-1} Na_2CO_3 showed high anodic production of H_2O_2, up to 3 mmol L^{-1} [43]. The working mechanism of Na_2SiO_3 as a H_2O_2 stabilizer is rather unclear. Literature reports for the stabilization mechanism include formation of complex between Na_2SiO_3 and H_2O_2 [70], formation of stable peroxide compounds, stopping the decomposition chain reactions by destruction of the free radicals, and formation of complexes with metal impurities [71]. Moreover, Na_2SiO_3 is also accounted for the stabilization of anodically produced peroxocarbonate species using BDD electrodes in Na_2CO_3 electrolytes [72]. However, the role of the metasilicate for H_2O oxidation to H_2O_2 has not been studied in depth.

We have investigated anolytes without and with Na_2SiO_3 and their effect on the anodic H_2O_2 generation. The addition of 30 mmol L^{-1} Na_2SiO_3 to the 2 mol L^{-1} $KHCO_3$ anolyte controlled at pH 9 caused a two-fold increase in H_2O_2 production: from 2.2 mmol L^{-1} to 4 mmol L^{-1} H_2O_2 (Fig. 7a). The maximum FE for H_2O_2 production increased from 1% to 4%, and the production rate increased fourfold (from 0.3 to 1.2 μmol min^{-1} cm^{-2}) (Supporting Information, Fig. S14a,b). Thus, the presence of Na_2SiO_3 in solution remarkably enhanced the formation and accumulation of H_2O_2 in the electrolyte.

The pH range of anolytes containing Na_2SiO_3 was varied from pH 8.4–14 in an H-cell at 50 mA cm^{-2}. This preliminary screening revealed higher production of H_2O_2 at elevated pH (> 9), with peak production of 300 μmol L^{-1} H_2O_2 at pH 11 (Fig. 7b). At pH above 11, the H_2O_2 production declined considerably, reaching 60 μmol L^{-1} at pH 14. Previous reports on anodic H_2O_2 production in different pHs show higher anodic H_2O_2 generation at pH below 11.4 [73]. In this study, the presence of Na_2SiO_3 inhibits H_2O_2 decomposition up to pH 11. At pH higher than 11, more stabilizer is required for increasing H_2O_2 concentrations (Supporting Information, Fig. S15a).

Experiments in the flow cell showed the same pattern: higher H_2O_2 concentrations were obtained in 2 mol L^{-1} $KHCO_3$ electrolytes containing Na_2SiO_3, even at higher pH (Fig. 7c). 26 mmol L^{-1} H_2O_2 was achieved at pH 12 in the presence of 90 mmol L^{-1} Na_2SiO_3, compared to 1.5 mmol L^{-1} at pH 8.4 without the stabilizer. These results suggest that higher pH enhances the electrochemical production of H_2O_2, provided that a chemical stabilizer hinders its subsequent decomposition.

Literature reports on anodic H_2O_2 production in different electrolytes and pH suggested that HCO_3^- ions promote H_2O_2 formation, whereas CO_3^{2-} ions aid to H_2O_2 decomposition [32]. K_2CO_3 electrolytes at pH 12.7 showed lower H_2O_2 production compared to other electrolytes with lower pH [74]. Regarding the pH variation, the Na_2SiO_3 stabilizer prevented H_2O_2 decomposition even in high alkaline conditions. Consequently, higher H_2O_2 concentrations were achieved at elevated pH. Calculations of $a(HCO_3^-)$ and $a(CO_3^{2-})$ in the electrolyte show a remarkable correspondence of higher H_2O_2 formation with higher $a(CO_3^{2-})$ upon pH variation (Fig. 7c).

To confirm the role of CO_3^{2-} ions on H_2O_2 production, K_2CO_3 electrolytes were utilized in the presence of Na_2SiO_3. K_2CO_3 electrolytes have been accounted for poor anodic production of H_2O_2 [74]. Nonetheless, we find considerably high H_2O_2 production upon increasing the Na_2SiO_3 concentration. An initial investigation in the H-Cell revealed higher stabilizer concentration results in high H_2O_2 production, particularly in high pH regimes (Supporting Information, Fig. S17). In the presence of 90 mol L^{-1} Na_2SiO_3, 33 mmol L^{-1} H_2O_2 was obtained after 150 min with a final FE of 14% (Fig. 7d), which is at least 20 times higher than the H_2O_2 concentration obtained in 2 mol L^{-1} $KHCO_3$ without the stabilizer. Thus, the influence of CO_3^{2-} ions is evident on the $2e^-$ oxidation of water to H_2O_2, as long as a chemical stabilizer is present to avoid peroxide decomposition.

3.6. Summary of work and proposed mechanism

Variation of $KHCO_3$ concentration in the anolyte revealed higher H_2O_2 production in more concentrated solutions. Literature reports proposed that the HCO_3^- ions oxidize to HCO_4^- during the anodic polarization (Eq. (16)). Subsequently, HCO_4^- decomposes to HCO_3^-, thereby releasing H_2O_2 (Eq. (17)) [37,43,46]. Therefore, HCO_3^- ions contribute to enhanced H_2O_2 formation.

However, increasing the $KHCO_3$ concentration results in a pH rise, which subsequently increases the activity of CO_3^{2-} ions due to the HCO_3^-/ CO_3^{2-} equilibrium. Our results of pH screening in 2 mol L^{-1} $KHCO_3$ are in agreement with the literature, showing that highly alkaline electrolytes are unfavorable for anodic H_2O_2 production [37]. Nevertheless, the addition of Na_2SiO_3 to the anolyte stabilized the H_2O_2 production even in pH regimes higher than 12. Changing the anolyte to 2 mol L^{-1} K_2CO_3 in the presence of Na_2SiO_3 at pH 12 confirmed the influence of the CO_3^{2-} ions activity in boosting H_2O_2 formation. A summary of the electrolyte optimization is given in Table 2, which shows an enhance in the anodic H_2O_2 production by a factor of 20 upon optimizing the electrolyte conditions.

Literature reports on anodic processes in carbonate electrolytes have shown that CO_3^{2-} ions can be oxidized to peroxodicarbonate ($C_2O_6^{2-}$) (Eq. (19)) [46,68,75]. Various carbon-based materials, including boron-doped diamond, have been accounted for producing peroxodicarbonate ions in solution [75–78]. Due to the poor stability of peroxocarbonate ions in aqueous solutions, it hydrolyses to form H_2O_2 and HCO_3^- (Eq. (20)) [68,72,78]. HCO_3^- ions are deprotonated to CO_3^{2-} at high pH, which consequently can undergo oxidation to $C_2O_6^{2-}$ (Eq. (7) and Fig. 8). We suggest a promotion effect of CO_3^{2-} ions in alkaline medium resulting in higher production of H_2O_2, provided a suitable amount of stabilizer is present in the electrolyte. *In situ* studies to identify the anodic generation of $C_2O_6^{2-}$ ions would be required to validate the peroxocarbonate mechanism.

$$2CO_3^{2-} \rightarrow C_2O_6^{2-} + 2e^- \; E^0 = 1.80 \text{ V vs. RHE} \quad (19)$$

$$C_2O_6^{2-} + 2H_2O \rightarrow H_2O_2 + 2HCO_3^- \quad (20)$$

The proposed crucial role of CO_3^{2-} ions in H_2O_2 formation is based on the activity profile of carbonate and bicarbonate ions and the H_2O_2 production at different pH values (Fig. 7c). At higher pH values, the chemical equilibrium of HCO_3^-/ CO_3^{2-} shifts to carbonate. Simultaneously, the H_2O_2 production increases, as long as a stabilizer is present to avoid H_2O_2 decomposition. Moreover, carbonate ions can be oxidized to peroxodicarbonate and release H_2O_2 via hydrolysis. In parallel to our investigations, the group of Gill et al. [63] demonstrated the role of carbonate in promoting anodic H_2O_2 production: first, a rotating ring disc electrode showed that H_2O_2 was not readily detected in the ring, but only with a time delay. This indicates oxidation of the electrolyte species followed by hydrolysis, thereby promoting H_2O_2 production. *In situ* infrared spectroscopy (ATR-FTIR) studies by the same group confirmed the role of carbonate and the presence of HCO_4^- or $C_2O_6^{2-}$ peroxo-intermediates on the electrode surface at the potentials of H_2O_2 generation [63]. In contrast to our results presented here, Gill et al. reported higher H_2O_2 productivity in HCO_3^- than in CO_3^{2-} electrolyte.

This difference lays in the use of stabilizers in our experiments. Chemical stabilizers enabled a superior reaction performance in higher pH regimes and higher CO_3^{2-} activities. The high pH of CO_3^{2-} solutions will lead to H_2O_2 decomposition in the absence of a stabilizer and consequently, a lower productivity compared to HCO_3^- solutions. DFT calculations by Mavrikis et al. also indicated an important role of CO_3^{2-} ions in enhancing the H_2O_2 production in an electrolyte mixture of 1:1 $KHCO_3$ and K_2CO_3, thus supporting our hypothesis [79].

A comparison of our results with those reported in the literature is summarized in Table 3. In this study, a maximum H_2O_2 concentration of 33 mmol L^{-1} was obtained, which is, to the best of our knowledge, the highest reported concentration of anodically produced H_2O_2 using CFP. Although the faradaic efficiency of 14.3% is not high, it is the highest FE obtained at such current density using pristine CFP [43]. The FE and the production rates, usually defined as performance parameters, are comparatively low and require further improvement by using foremost active electrode materials. Nonetheless, it is important to point out that we have used a low-cost, readily available carbon material as a working electrode. Additionally, a comparatively more significant 10 cm^2 flow cell and higher electrolyte volume have been utilized in this study to demonstrate improvements in the H_2O_2 accumulation by optimizing the electrolyte composition and operating conditions.

4. Conclusion

The performance of low-cost commercial carbon materials as anodes for anodic H_2O_2 production was investigated through variation and optimization of a broad range of electrolyte composition and operating parameters. We showed that carbon fiber paper exhibited good selectivity toward water oxidation to H_2O_2 and used it for further in-depth examinations. This study highlights the importance of tuning reaction conditions such as potential, current density, electrolyte concentrations, pH values, and utilization of stabilizer to boost the electrochemical water oxidation to H_2O_2. Supported by the calculated activity of carbonate species in the electrolyte, the experimental data suggested a strong correlation between the $a(CO_3^{2-})$ and enhanced H_2O_2 generation in $KHCO_3$ anolytes. Keeping the activity of CO_3^{2-} ions high by regulating the pH regime to remain stable at 9 almost doubled the H_2O_2 production, reaching 2.2 mmol L^{-1}. Thus, CO_3^{2-} does not compete, but acts as a reaction mediator promoting H_2O_2 production. Adding Na_2SiO_3 to the electrolyte as a stabilizer remarkably boosted the anodic generation of H_2O_2 at higher pH regimes·H_2O_2 concentration up to 26 mmol L^{-1} was obtained in 2 mol L^{-1} $KHCO_3$ at pH 12. Finally, this study illustrated the importance of suitable electrolyte conditions for improving the electrochemical oxidation of water to H_2O_2. Optimized electrolyte conditions (90 mmol L^{-1} Na_2SiO_3 in 2 mol L^{-1} K_2CO_3) led to H_2O_2 concentrations up to 33 mmol L^{-1}, at least 20 fold higher than in 2 mol L^{-1} $KHCO_3$, which is used as a standard electrolyte. Future approaches will emphasize the optimized electrolyte condition with highly active electrode materials to enhance the anodic production of H_2O_2. This is subject to our ongoing work.

CRediT authorship contribution statement

Dhananjai Pangotra: Conceptualization, Investigation, Formal analysis, Validation, Writing – original. draft. **Lénárd-István Csepei:** Conceptualization, Writing – review & editing. **Arne Roth:** Conceptualization, Supervision, Writing – review & editing. **Carlos Ponce de León:** Writing – review & editing. **Volker Sieber:** Supervision, Writing – review & editing. **Luciana Vieira:** Conceptualization, Supervision, Writing – review & editing.

Declaration of Competing Interest

The authors declare that they have no known competing financial interests or personal relationships that could have appeared to influence the work reported in this paper.

Acknowledgements

The authors thank Prof. Cordt Zollfrank (TUM-CS) for allowing using the SEM. Annette Weiske and Manuela Kaiser are deeply acknowledged for their technical support. Dr. Sumanth Ranganathan (SCION, New Zealand) is acknowledged for fruitful scientific discussions. We thank Sotirios Mavrikis (University of Southampton) and Johanna Radomski (TUM-CS) for reading the manuscript and providing feedback. The authors express their gratitude to the European Commission for the financial support of this research within the European Framework Programme for Research and Innovation Horizon 2020 (CO2EXIDE, Grant No. 768789).

Appendix A. Supporting information

Supplementary data associated with this article can be found in the online version at doi:10.1016/j.apcatb.2021.120848.

References

[1] C.P. Gordon, H. Engler, A.S. Tragl, M. Plodinec, T. Lunkenbein, A. Berkessel, J. H. Teles, A.-N. Parvulescu, C. Copéret, Efficient epoxidation over dinuclear sites in titanium silicalite-1, Nature 586 (2020) 708–713, https://doi.org/10.1038/s41586-020-2826-3.

[2] A. Pokutsa, A. Zaborovsky, P. Bloniarz, T. Pacześniak, D. Maksym, J. Muzart, Cyclohexane oxidation: relationships of the process efficiency with electrical conductance, electronic and cyclic voltammetry spectra of the reaction mixture, React. Kinet. Mech. Catal. 132 (2021) 123–137, https://doi.org/10.1007/s11144-020-01913-6.

[3] G. Lewandowski, M. Kujbida, A. Wróblewska, Epoxidation of 1,5,9-cyclododecatriene with hydrogen peroxide under phase-transfer catalysis conditions: influence of selected parameters on the course of epoxidation, React. Kinet. Mech. Catal. 132 (2021) 983–1001, https://doi.org/10.1007/s11144-021-01960-7.

[4] D. Horová, J. Nováková, L. Pelíšková, J. Kohout, J. Šafář, K. Hrachovcová, V. Tokarová, Synthesis of MFI structured iron silicates and their catalytic performance in phenol removal by wet peroxide oxidation, React. Kinet. Mech. Catal. 130 (2020) 1077–1092, https://doi.org/10.1007/s11144-020-01804-w.

[5] İ. Kıpçak, E.Kurtaran Ersal, Catalytic wet peroxide oxidation of a real textile azo dye Cibacron Red P-4B over Al/Fe pillared bentonite catalysts: kinetic and thermodynamic studies, React. Kinet. Mech. Catal. 132 (2021) 1003–1023, https://doi.org/10.1007/s11144-021-01962-5.

[6] A.S. Gohardani, J. Stanojev, A. Demairé, K. Anflo, M. Persson, N. Wingborg, C. Nilsson, Green space propulsion: opportunities and prospects, Prog. Aerosp. Sci. 71 (2014) 128–149, https://doi.org/10.1016/j.paerosci.2014.08.001.

[7] S.C. Perry, D. Pangotra, L. Vieira, L.-I. Csepei, V. Sieber, L. Wang, C. Ponce de León, F.C. Walsh, Electrochemical synthesis of hydrogen peroxide from water and oxygen, Nat. Rev. Chem. 3 (2019) 442–458, https://doi.org/10.1038/s41570-019-0110-6.

[8] ISRO working on green fuels like hydrogen peroxide for rockets, The Economic Times Chennai, 2020. ⟨https://energy.economictimes.indiatimes.com/news/renewable/isro-working-on-green-fuels-like-hydrogen-peroxide-for-rockets/80045159⟩. (Accessed 2 January 2021).

[9] J.M. Ramos, J.A. Wang, S.O. Flores, L.F. Chen, N. Nava, J. Navarrete, J. M. Domínguez, J.A. Szpunar, Ultrasound-assisted synthesis and catalytic activity of mesostructured FeOx/SBA-15 and FeOx/Zr-SBA-15 catalysts for the oxidative desulfurization of model diesel, Catal. Today 349 (2020) 198–209, https://doi.org/10.1016/j.cattod.2018.04.059.

[10] F. Bibak, G. Moradi, Oxidative desulfurization of model oil and oil cuts with MoO_3/SBA-15: experimental design and optimization by Box–Behnken method, React. Kinet. Mech. Catal. 131 (2020) 935–951, https://doi.org/10.1007/s11144-020-01852-2.

[11] T.A.G. Duarte, S.M.G. Pires, I.C.M.S. Santos, M.M.Q. Simões, M.G.P.M.S. Neves, A. M.V. Cavaleiro, J.A.S. Cavaleiro, A Mn(iii) polyoxotungstate in the oxidation of organosulfur compounds by H_2O_2 at room temperature: an environmentally safe catalytic approach, Catal. Sci. Technol. 6 (2016) 3271–3278, https://doi.org/10.1039/c5cy01564b.

[12] R. Ghubayra, C. Nuttall, S. Hodgkiss, M. Craven, E.F. Kozhevnikova, I. V. Kozhevnikov, Oxidative desulfurization of model diesel fuel catalyzed by carbon-supported heteropoly acids, Appl. Catal. B Environ. 253 (2019) 309–316, https://doi.org/10.1016/j.apcatb.2019.04.063.

[13] J.S.J. Hargreaves, Y.-M. Chung, W.-S. Ahn, T. Hisatomi, K. Domen, M.C. Kung, H. H. Kung, Minimizing energy demand and environmental impact for sustainable NH_3 and H_2O_2 production—a perspective on contributions from thermal, electro-, and photo-catalysis, Appl. Catal. A Gen. 594 (2020), 117419, https://doi.org/10.1016/j.apcata.2020.117419.

[14] J. Casey, IMO 2020 to impact European refineries, Hydrocarbon Engineering, 2020. ⟨https://www.hydrocarbonengineering.com/clean-fuels/20012020/imo-2020-to-impact-european-refineries/⟩. (Accessed 28 December 2020).

[15] A. Halff, L. Younes, T. Boersma, The likely implications of the new IMO standards on the shipping industry, Energy Policy 126 (2019) 277–286, https://doi.org/10.1016/j.enpol.2018.11.033.

[16] T.P.V. Zis, K. Cullinane, The desulphurisation of shipping: past, present and the future under a global cap, Transp. Res. D Transp. Environ. 82 (2020), 102316, https://doi.org/10.1016/j.trd.2020.102316.

[17] E. Linley, S.P. Denyer, G. McDonnell, C. Simons, J.Y. Maillard, Use of hydrogen peroxide as a biocide: new consideration of its mechanisms of biocidal action, J. Antimicrob. Chemother. 67 (2012) 1589–1596, https://doi.org/10.1093/jac/dks129.

[18] J. Andrew Kielbania, Anti-microbial composition and method for making and using same, Bioneutral Laboratories Corporation, 2015.

[19] WHO-recommended handrub formulations, WHO Guidelines on Hand Hygiene in Health Care: First Global Patient Safety Challenge Clean Care Is Safer Care, WHO Press, 2009. ⟨https://www.ncbi.nlm.nih.gov/books/NBK144054/⟩. (Accessed 5 January 2021).

[20] J.C. Rubio-Romero, M.D.C. Pardo-Ferreira, J.A. Torrecilla-Garcia, S. Calero-Castro, Disposable masks: disinfection and sterilization for reuse, and non-certified manufacturing, in the face of shortages during the COVID-19 pandemic, Saf. Sci. 129 (2020), 104830, https://doi.org/10.1016/j.ssci.2020.104830.

[21] V. Saini, K. Sikri, S.D. Batra, P. Kalra, K. Gautam, Development of a highly effective low-cost vaporized hydrogen peroxide-based method for disinfection of personal protective equipment for their selective reuse during pandemics, Gut Pathog. 12 (2020) 29, https://doi.org/10.1186/s13099-020-00367-4.

[22] V.C.C. Cheng, S.C. Wong, G.S.W. Kwan, W.T. Hui, K.Y. Yuen, Disinfection of N95 respirators by ionized hydrogen peroxide during pandemic coronavirus disease 2019 (COVID-19) due to SARS-CoV-2, J. Hosp. Infect. 105 (2020) 358–359, https://doi.org/10.1016/j.jhin.2020.04.003.

[23] Hydrogen peroxide demand rises in battle against COVID-19, Hydrogen Peroxide: COVID-19, Research and Markets, 2020. ⟨https://www.researchandmarkets.com/issues/hydrogen-peroxide-demand-rises⟩. (Accessed 13 May 2021).

[24] G.P. Riedl H.-J, Production of Hydrogen Peroxide, 1939.

[25] S. Anantharaj, S. Pitchaimuthu, S. Noda, A review on recent developments in electrochemical hydrogen peroxide synthesis with a critical assessment of perspectives and strategies, Adv. Colloid Interface Sci. 287 (2021), 102331, https://doi.org/10.1016/j.cis.2020.102331.

[26] C.P. De Leon, D. Pletcher, Removal of formaldehyde from aqueous solutions via oxygen reduction using a reticulated vitreous carbon cathode cell, J. Appl. Electrochem. 25 (1995) 307–314, https://doi.org/10.1007/bf00249648.

[27] P.J.M. Cordeiro-Junior, M.S. Kronka, L.A. Goulart, N.C. Veríssimo, L.H. Mascaro, M.Cd Santos, R. Bertazzoli, M.Rd.V. Lanza, Catalysis of oxygen reduction reaction for H_2O_2 electrogeneration: the impact of different conductive carbon matrices and their physicochemical properties, J. Catal. 392 (2020) 56–68, https://doi.org/10.1016/j.jcat.2020.09.020.

[28] R.S. Rocha, R.B. Valim, L.C. Trevelin, J.R. Steter, J.F. Carneiro, J.C. Forti, R. Bertazzoli, M.R.V. Lanza, Electrocatalysis of hydrogen peroxide generation using oxygen-fed gas diffusion electrodes made of carbon black modified with quinone compounds, Electrocatalysis 11 (2020) 338–346, https://doi.org/10.1007/s12678-020-00591-1.

[29] J. Moreira, V. Bocalon Lima, L. Athie Goulart, M.R.V. Lanza, Electrosynthesis of hydrogen peroxide using modified gas diffusion electrodes (MGDE) for environmental applications: quinones and azo compounds employed as redox modifiers, Appl. Catal. B Environ. 248 (2019) 95–107, https://doi.org/10.1016/j.apcatb.2019.01.071.

[30] G.V. Fortunato, E. Pizzutilo, E.S.F. Cardoso, M.R.V. Lanza, I. Katsounaros, S. J. Freakley, K.J.J. Mayrhofer, G. Maia, M. Ledendecker, The oxygen reduction reaction on palladium with low metal loadings: the effects of chlorides on the stability and activity towards hydrogen peroxide, J. Catal. 389 (2020) 400–408, https://doi.org/10.1016/j.jcat.2020.06.019.

[31] A. Verdaguer-Casadevall, D. Deiana, M. Karamad, S. Siahrostami, P. Malacrida, T. W. Hansen, J. Rossmeisl, I. Chorkendorff, I.E. Stephens, Trends in the electrochemical synthesis of H_2O_2: enhancing activity and selectivity by electrocatalytic site engineering, Nano Lett. 14 (2014) 1603–1608, https://doi.org/10.1021/nl500037x.

[32] K. Fuku, Y. Miyase, Y. Miseki, T. Funaki, T. Gunji, K. Sayama, Photoelectrochemical hydrogen peroxide production from water on a WO_3 /$BiVO_4$ photoanode and from O_2 on an Au cathode without external bias, Chem. Asian J. 12 (2017) 1111–1119, https://doi.org/10.1002/asia.201700292.

[33] H. Li, P. Wen, D.S. Itanze, Z.D. Hood, S. Adhikari, C. Lu, X. Ma, C. Dun, L. Jiang, D. L. Carroll, Y. Qiu, S.M. Geyer, Scalable neutral H_2O_2 electrosynthesis by platinum diphosphide nanocrystals by regulating oxygen reduction reaction pathways, Nat. Commun. 11 (2020) 3928, https://doi.org/10.1038/s41467-020-17584-9.

[34] F. Ma, S. Wang, X. Liang, C. Wang, F. Tong, Z. Wang, P. Wang, Y. Liu, Y. Dai, Z. Zheng, B. Huang, Ni_3B as a highly efficient and selective catalyst for the electrosynthesis of hydrogen peroxide, Appl. Catal. B Environ. 279 (2020), 119371, https://doi.org/10.1016/j.apcatb.2020.119371.

[35] J.F. Pérez, J. Llanos, C. Sáez, C. López, P. Cañizares, M.A. Rodrigo, Towards the scale up of a pressurized-jet microfluidic flow-through reactor for cost-effective electro-generation of H_2O_2, J. Clean. Prod. 211 (2019) 1259–1267, https://doi.org/10.1016/j.jclepro.2018.11.225.

[36] J.F. Pérez, J. Llanos, C. Sáez, C. López, P. Cañizares, M.A. Rodrigo, On the design of a jet-aerated microfluidic flow-through reactor for wastewater treatment by electro-Fenton, Sep. Purif. Technol. 208 (2019) 123–129, https://doi.org/10.1016/j.seppur.2018.04.021.

[37] K. Fuku, K. Sayama, Efficient oxidative hydrogen peroxide production and accumulation in photoelectrochemical water splitting using a tungsten trioxide/bismuth vanadate photoanode, Chem. Commun. 52 (2016) 5406–5409, https://doi.org/10.1039/c6cc01605g.

[38] X. Shi, S. Siahrostami, G.L. Li, Y. Zhang, P. Chakthranont, F. Studt, T.F. Jaramillo, X. Zheng, J.K. Norskov, Understanding activity trends in electrochemical water oxidation to form hydrogen peroxide, Nat. Commun. 8 (2017) 701, https://doi.org/10.1038/s41467-017-00585-6.

[39] S.Y. Park, H. Abroshan, X. Shi, H.S. Jung, S. Siahrostami, X. Zheng, $CaSnO_3$: an electrocatalyst for two-electron water oxidation reaction to form H_2O_2, ACS Energy Lett. 4 (2018) 352–357, https://doi.org/10.1021/acsenergylett.8b02303.

[40] T. Kang, B. Li, Q. Hao, W. Gao, F. Bin, K.N. Hui, D. Fu, B. Dou, Efficient hydrogen peroxide (H_2O_2) synthesis by $CaSnO_3$ via two-electron water oxidation reaction, ACS Sustain. Chem. Eng. 8 (2020) 15005–15012, https://doi.org/10.1021/acssuschemeng.0c05449.

[41] K. Fuku, Y. Miyase, Y. Miseki, T. Gunji, K. Sayama, Enhanced oxidative hydrogen peroxide production on conducting glass anodes modified with metal oxides, ChemistrySelect 1 (2016) 5721–5726, https://doi.org/10.1002/slct.201601469.

[42] S.R. Kelly, X. Shi, S. Back, L. Vallez, S.Y. Park, S. Siahrostami, X. Zheng, J. K. Nørskov, ZnO as an active and selective catalyst for electrochemical water oxidation to hydrogen peroxide, ACS Catal. 9 (2019) 4593–4599, https://doi.org/10.1021/acscatal.8b04873.

[43] C. Xia, S. Back, S. Ringe, K. Jiang, F. Chen, X. Sun, S. Siahrostami, K. Chan, H. Wang, Confined local oxygen gas promotes electrochemical water oxidation to hydrogen peroxide, Nat. Catal. 3 (2020) 125–134, https://doi.org/10.1038/s41929-019-0402-8.

[44] S. Mavrikis, M. Göltz, S. Rosiwal, L. Wang, C. Ponce de León, Boron-Doped diamond electrocatalyst for enhanced anodic H_2O_2 production, ACS Appl. Energy Mater. 3 (2020) 3169–3173, https://doi.org/10.1021/acsaem.0c00093.

[45] X. Shi, S. Back, T.M. Gill, S. Siahrostami, X. Zheng, Electrochemical synthesis of H_2O_2 by two-electron water oxidation reaction, Chem 7 (2021) 38–63, https://doi.org/10.1016/j.chempr.2020.09.013.

[46] S. Mavrikis, S.C. Perry, P.K. Leung, L. Wang, C. Ponce de León, Recent advances in electrochemical water oxidation to produce hydrogen peroxide: a mechanistic perspective, ACS Sustain. Chem. Eng. 9 (2020) 76–91, https://doi.org/10.1021/acssuschemeng.0c07263.

[47] C. Xia, Y. Xia, P. Zhu, L. Fan, H. Wang, Direct electrosynthesis of pure aqueous H_2O_2 solutions up to 20% by weight using a solid electrolyte, Science 366 (2019) 226–231, https://doi.org/10.1126/science.aay1844.

[48] N. Gurieff, D. Green, I. Koskinen, M. Lipson, M. Baldry, A. Maddocks, C. Menictas, J. Noack, B. Moghtaderi, E. Doroodchi, Healthy power: reimagining hospitals as sustainable energy hubs, Sustainability 12 (2020) 8554, https://doi.org/10.3390/su12208554.

[49] A. Siddharta, S. Pfaender, N.J. Vielle, R. Dijkman, M. Friesland, B. Becker, J. Yang, M. Engelmann, D. Todt, M.P. Windisch, F.H. Brill, J. Steinmann, J. Steinmann, S. Becker, M.P. Alves, T. Pietschmann, M. Eickmann, V. Thiel, E. Steinmann, Virucidal activity of world health organization-recommended formulations against enveloped viruses, including Zika, Ebola, and emerging coronaviruses, J. Infect. Dis. 215 (2017) 902–906, https://doi.org/10.1093/infdis/jix046.

[50] G. Kampf, D. Todt, S. Pfaender, E. Steinmann, Persistence of coronaviruses on inanimate surfaces and their inactivation with biocidal agents, J. Hosp. Infect. 104 (2020) 246–251, https://doi.org/10.1016/j.jhin.2020.01.022.

[51] J.P. Wood, W. Richter, M. Sunderman, M.W. Calfee, S. Serre, L. Mickelsen, Evaluating the environmental persistence and inactivation of MS_2 bacteriophage and the presumed Ebola virus surrogate Phi6 using low concentration hydrogen peroxide vapor, Environ. Sci. Technol. 54 (2020) 3581–3590, https://doi.org/10.1021/acs.est.9b06034.

[52] I. Salmerón, K.V. Plakas, I. Sirés, I. Oller, M.I. Maldonado, A.J. Karabelas, S. Malato, Optimization of electrocatalytic H_2O_2 production at pilot plant scale for solar-assisted water treatment, Appl. Catal. B Environ. 242 (2019) 327–336, https://doi.org/10.1016/j.apcatb.2018.09.045.

[53] L. Li, Z. Hu, J.C. Yu, On-demand synthesis of H_2O_2 by water oxidation for sustainable resource production and organic pollutant degradation, Angew. Chem. Int. Ed. Engl. 59 (2020) 20538–20544, https://doi.org/10.1002/anie.202008031.

[54] Y. Jin, Y. Shi, Z. Chen, R. Chen, X. Chen, X. Zheng, Y. Liu, R. Ding, Enhancement of solar water disinfection using H_2O_2 generated in situ by electrochemical reduction, Appl. Catal. B Environ. 267 (2020), 118730, https://doi.org/10.1016/j.apcatb.2020.118730.

[55] G. Ferro, A. Fiorentino, M.C. Alferez, M.I. Polo-López, L. Rizzo, P. Fernández-Ibáñez, Urban wastewater disinfection for agricultural reuse: effect of solar driven AOPs in the inactivation of a multidrug resistant E. coli strain, Appl. Catal. B Environ. 178 (2015) 65–73, https://doi.org/10.1016/j.apcatb.2014.10.043.

[56] T.M. Gill, X. Zheng, Comparing methods for quantifying electrochemically accumulated H_2O_2, Chem. Mater. 32 (2020) 6285–6294, https://doi.org/10.1021/acs.chemmater.0c02010.

[57] S. Ranganathan, V. Sieber, Development of semi-continuous chemo-enzymatic terpene epoxidation: combination of anthraquinone autooxidation and the lipase-mediated epoxidation process, React. Chem. Eng. 2 (2017) 885–895, https://doi.org/10.1039/c7re00112f.

[58] E.N. Kadnikova, N.M. Kostić, Oxidation of ABTS by hydrogen peroxide catalyzed by horseradish peroxidase encapsulated into sol–gel glass, J. Mol. Catal. B Enzym. 18 (2002) 39–48, https://doi.org/10.1016/s1381-1177(02)00057-7.

[59] S. Hrn, dm. Mn, K. Ac, Status of hydrogen peroxide solution 10 V in commercialized samples, Pharm. Anal. Acta 8 (2017), https://doi.org/10.4172/2153-2435.1000567.
[60] O. Pedersen, T.D. Colmer, K. Sand-Jensen, Underwater photosynthesis of submerged plants - recent advances and methods, Front. Plant Sci. 4 (2013) 140, https://doi.org/10.3389/fpls.2013.00140.
[61] D.E. Richardson, H. Yao, K.M. Frank, D.A. Bennett, Equilibria, kinetics, and mechanism in the bicarbonate activation of hydrogen peroxide: oxidation of sulfides by peroxymonocarbonate, J. Am. Chem. Soc. 122 (2000) 1729–1739, https://doi.org/10.1021/ja9927467.
[62] A. El-kharouf, B.G. Pollet, Chapter 4 - gas diffusion media and their degradation, in: M.M. Mench, E.C. Kumbur, T.N. Veziroglu (Eds.), Polymer Electrolyte Fuel Cell Degradation, Academic Press, Boston, 2012, pp. 215–247, https://doi.org/10.1016/B978-0-12-386936-4.10004-1.
[63] T.M. Gill, L. Vallez, X. Zheng, The role of bicarbonate-based electrolytes in H_2O_2 production through two-electron water oxidation, ACS Energy Lett. 6 (2021) 2854–2862, https://doi.org/10.1021/acsenergylett.1c01264.
[64] Y. Yi, G. Weinberg, M. Prenzel, M. Greiner, S. Heumann, S. Becker, R. Schlögl, Electrochemical corrosion of a glassy carbon electrode, Catal. Today 295 (2017) 32–40, https://doi.org/10.1016/j.cattod.2017.07.013.
[65] H. Schultz, G. Bauer, E. Schachl, F. Hagedorn, P. Schmittinger, Potassium Compounds, Ullmann's Encyclopedia of Industrial Chemistry. ⟨https://doi.org/10.1002/14356007.a22_039⟩.
[66] P.A. Michaud, Electrochemical oxidation of water on synthetic boron-doped diamond thin film anodes, J. Appl. Electrochem. 33 (2003) 151–154, https://doi.org/10.1023/a:1024084924058.
[67] H. Lee, A.-H. Park, C. Oloman, Stability of hydrogen peroxide in sodium carbonate solutions, Tappi J. 83 (2000).
[68] J. Zhang, C.W. Oloman, Electro-oxidation of carbonate in aqueous solution on a platinum rotating ring disk electrode, J. Appl. Electrochem. 35 (2005) 945–953, https://doi.org/10.1007/s10800-005-7078-2.
[69] A.O. Terent'ev, Z.Y. Pastukhova, I.A. Yaremenko, L.G. Bruk, G.I. Nikishin, Promising hydrogen peroxide stabilizers for large-scale application: unprecedented effect of aryl alkyl ketones, Mendeleev Commun. 26 (2016) 329–331, https://doi.org/10.1016/j.mencom.2016.07.021.
[70] K. Hanna, Comment on "Inhibitory effect of dissolved silica on H_2O_2 decomposition by iron(III) and manganese(IV) oxides: implications for H_2O_2–based in situ chemical oxidation", Environ. Sci. Technol. 46 (2012) 3591–3592, https://doi.org/10.1021/es3002103.
[71] I. Charron, A. Couvert, A. Laplanche, C. Renner, L. Patria, B. Requieme, Treatment of odorous sulphur compounds by chemical scrubbing with hydrogen peroxide - stabilisation of the scrubbing solution, Environ. Sci. Technol. 40 (2006) 7881–7885, https://doi.org/10.1021/es060414d.
[72] E.J. Ruiz-Ruiz, Y. Meas, R. Ortega-Borges, J.L.Jurado Baizabal, Electrochemical production of peroxocarbonate at room temperature using conductive diamond anodes, Surf. Eng. Appl. Electrochem. 50 (2015) 478–484, https://doi.org/10.3103/S106837551406009X.
[73] F. Kuttassery, A. Sebastian, S. Mathew, H. Tachibana, H. Inoue, Promotive effect of bicarbonate ion on two-electron water oxidation to form H_2O_2 catalyzed by aluminum porphyrins, ChemSusChem 12 (2019) 1939–1948, https://doi.org/10.1002/cssc.201900560.
[74] W.D. Nicoll, A.F. Smith, Stability of dilute alkaline solutions of hydrogen peroxide, Ind. Eng. Chem. 47 (1955) 2548–2554, https://doi.org/10.1021/ie50552a051.
[75] S. Lips, S.R. Waldvogel, Use of boron-doped diamond electrodes in electro-organic synthesis, ChemElectroChem 6 (2019) 1649–1660, https://doi.org/10.1002/celc.201801620.
[76] P.Mvd Wiel, L.J.J. Janssen, J.G. Hoogland, Electrolysis of a carbonate-borate solution with a platinum anode—I. Current efficiency at perborate concentration of zero, Electrochim. Acta 16 (1971) 1217–1226, https://doi.org/10.1016/0013-4686(71)85110-1.
[77] C.P. Chardon, T. Matthée, R. Neuber, M. Fryda, C. Comninellis, Efficient electrochemical production of peroxodicarbonate applying DIACHEM®Diamond electrodes, ChemistrySelect 2 (2017) 1037–1040, https://doi.org/10.1002/slct.201601583.
[78] R.R.Rais Irkham, T.A. Ivandini, A. Fiorani, Y. Einaga, Electrogenerated chemiluminescence of luminol mediated by carbonate electrochemical oxidation at a boron-doped diamond, Anal. Chem. 93 (2021) 2336–2341, https://doi.org/10.1021/acs.analchem.0c04212.
[79] S. Mavrikis, M. Göltz, S.C. Perry, F. Bogdan, P.K. Leung, S. Rosiwal, L. Wang, C. Ponce de León, Effective hydrogen peroxide production from electrochemical water oxidation, ACS Energy Lett. 6 (2021) 2369–2377, https://doi.org/10.1021/acsenergylett.1c00904.
[80] K. Wenderich, B.A.M. Nieuweweme, G. Mul, B.T. Mei, Selective electrochemical oxidation of H_2O to H_2O_2 using boron-doped diamond: an experimental and techno-economic evaluation, ACS Sustain. Chem. Eng. 9 (2021) 7803–7812, https://doi.org/10.1021/acssuschemeng.1c01244.